Quantitative Measurements of Vibration Amplitude Using a Contact-Mode Freestanding Triboelectric Nanogenerator

Sihong Wang,[†] Simiao Niu,[†] Jin Yang,[†] Long Lin,[†] and Zhong Lin Wang*[,†,‡]

[†]School of Materials Science and Engineering, Georgia Institute of Technology, Atlanta, Georgia 30332-0245, United States, and [‡]Beijing Institute of Nanoenergy and Nanosystems, Chinese Academy of Sciences, Beijing 100083, China

ABSTRACT A vibration sensor is usually designed to measure the vibration frequency but disregard the vibration amplitude, which is rather challenging to be quantified due to the requirement of linear response. Here, we show the application of triboelectric nanogenerator (TENG) as a self-powered tool for quantitative measurement of vibration amplitude based on an operation mode, the contact-mode freestanding triboelectric nanogenerator (CF-TENG). In this mode, the triboelectrically charged resonator can be agitated to vibrate between two stacked stationary electrodes. Under the working principle with a constant capacitance between two electrodes, the amplitudes of the electric signals are proportional to the vibration amplitude of the resonator (provided that the resonator plate is charged to saturation), which has been illuminated both theoretically and experimentally. Together with its capability in monitoring the vibration frequency, the CF-TENG appears as the triboelectrification-based active sensor that can give full quantitative information about a vibration. In addition, the CF-TENG is also demonstrated as a power source for electronic devices.

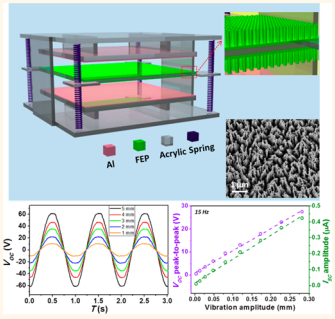

KEYWORDS: vibration · self-powered active sensors · quantitative sensing · triboelectric nanogenerators · mechanical energy harvesting

Vibration is one of the most important and ubiquitous forms of mechanical motions in people's living environment, which can be generated by a variety of different sources, such as machineries, running vehicles, infrastructures (*e.g.*, buildings, bridges), and even ocean waves. These vibrations are not only a potential energy resource to be utilized by human beings,[1−4] but more importantly, they can directly reflect the operation status and conditions of machineries and infrastructures.[5−10] Generally, vibrations are characterized by two parameters: frequency and amplitude. The vibration frequency can be easily quantified by most vibration sensors, but a quantitative measurement of the amplitude is relatively more difficult because it often requires a linear relationship between the sensing signal and the amplitude especially considering the requirement of most post signal processing systems. In recent years, the development of triboelectric nanogenerators (TENGs)[11−18] based on the conjunction of contact-electrification[19−21] and electrostatic induction has provided a highly feasible and practical approach for realizing self-powered active sensing for mechanical stimulus,[22,23] including vibrations. However, the several demonstrated TENG structures for vibration applications based on the vertical contact-separation mode is only applicable for measuring the frequency but not the amplitude.[24−29] This is because the electricity generation behavior of the vertical contact-separation mode is not linear to the separation distance, due to the nature of the changing capacitance between the two electrodes during its operation.[30] Therefore, in order to develop TENG-based self-powered sensor for quantifying the vibration amplitude, it is highly desirable to establish a TENG operation mode with constant capacitance between the electrodes (*i.e.*, stationary electrodes) and confined electric field during the operation.

Recently, a new fundamental mode of TENG—freestanding triboelectric layer mode

* Address correspondence to zlwang@gatech.edu.

Received for review September 25, 2014 and accepted November 7, 2014.

Published online 10.1021/nn5054365

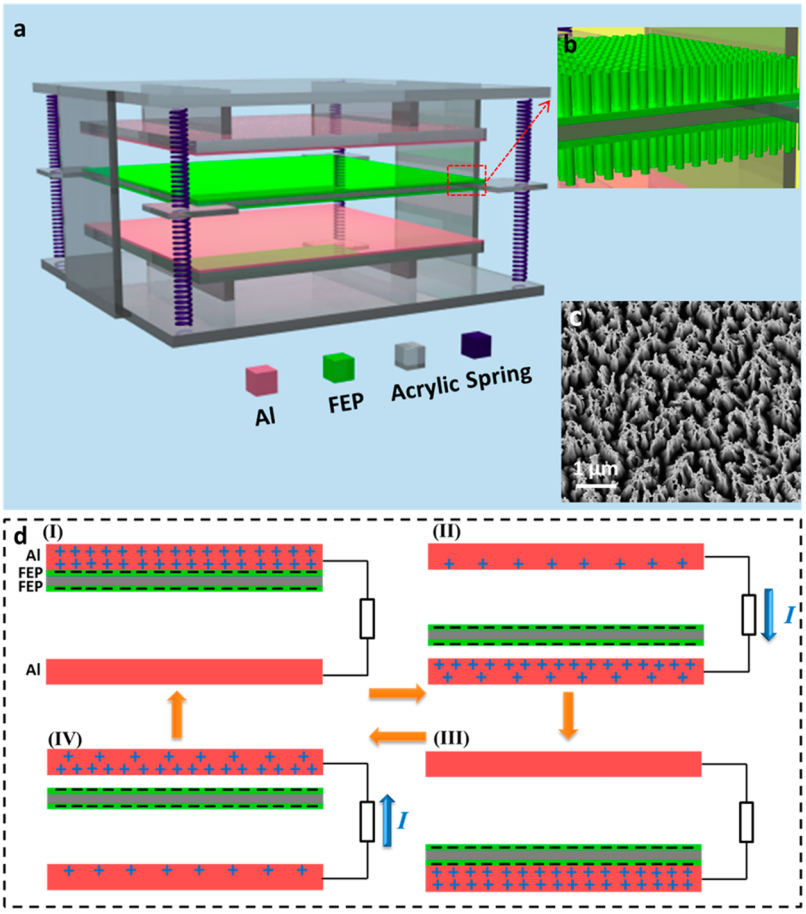

Figure 1. Device structure and working principle of the contact-mode freestanding triboelectric layer based nanogenerator (CF-TENG). (a) Schematic diagram showing the typical device structure of a CF-TENG. (b) Enlarged view of the device structure showing the nanowire-structure on the surface of the FEP films attached on the resonator plate. (c) SEM image of the nanowire structures on the FEP films. (d) Schematic diagram showing the basic working principle of the CF-TENG.

has been proposed, in which two stationary electrodes sit on the same plane and an electrode-free triboelectric layer cyclically slides between their surfaces.[17] This new fundamental mode of TENG offers several distinctive advantages for practical applications, such as electrode-free structure for harvesting energy from any arbitrary moving object, and the non-contact operation that helps to achieve an extremely high total conversion efficiency (as high as 85% for low frequency human motion) and a supreme stability.[17,31,32] More importantly, the capacitance between the electrodes remains constant during the operation. Parallel to the previous demonstrations on the freestanding-TENGs that are all based on the sliding-induced in-plane charge separation, this fundamental mode can also be realized by a vertical contact-separation operation with a stacked configuration, which can help to confine the electric field within the space between the two electrodes and thus lead to a linear electricity generation behavior. In this paper, we demonstrated a contact-mode freestanding-TENG (CF-TENG), in which the vibration of the freestanding triboelectric layer between the two electrodes periodically changes the induced potential difference between the two electrodes and thus generates electricity in external load. In such a structure with the electrodes' lateral dimension much larger than their vertical separation distance, the electricity generation has a linear relationship with the moving distance of the freestanding layer. On the basis of this unique linearity both theoretically and experimentally revealed in this paper, the CF-TENG is developed as the triboelectrification-enabled self-powered vibration sensor that can quantitatively measure both the vibration amplitude and frequency. Additionally, the CF-TENG is also demonstrated as an effective energy harvester for vibration with the capability of non-contact operation.

RESULTS AND DISCUSSION

The structural design of the vibration-enabled CF-TENG is schematically shown in Figure 1a. Its skeleton is constructed by laser-cut acrylic sheets. Two Al-deposited acrylic plates are supported in a face-to-face configuration with a distance of 2 cm, which serve as the two stationary electrodes of the CF-TENG. They both have a lateral dimension of 10 cm. In between, another acrylic sheet (with the thickness of ~1.6 mm) is employed as the vibration resonator in the CF-TENG

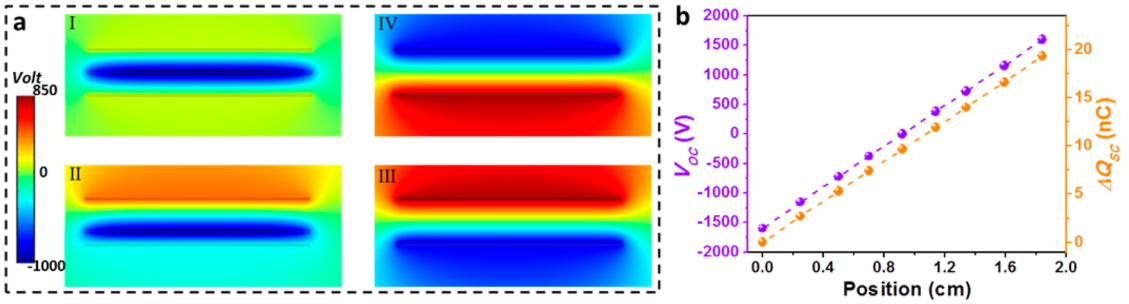

Figure 2. Numerical simulation results showing the characteristics of the CF-TENG's electricity generation behavior. (a) Simulated potential distributions of the CF-TENG at the open-circuit condition, with the resonator plate at four different positions. (b) Simulated open-circuit voltages (V_{OC}) and short-circuit charge densities (ΔQ_{SC}) of the CF-TENG at different positions (x) of the resonator plate.

through having its four corners connected by 8 springs (all with the spring constant of 33.3 N/m) to the two ends of the acrylic skeleton. Two 50-μm fluorinated ethylene propylene (FEP) films that are purposely chosen as the freestanding triboelectric layers due to their distinctively opposite triboelectric polarity with Al are laminated onto the two sides of this acrylic sheet. They have the same size with the electrode. Triggered by the external vibration source to which the CF-TENG is attached, the two triboelectric layers are brought by the resonating acrylic sheet to alternatively approach the two electrodes in a vertical-to-plane manner. When its vibration amplitude is large enough, the contact between the FEP layer and the Al surface will generate triboelectric charges. Since the FEP is an electret material, the triboelectric charges can preserve on its surface for a very long time to induce the electricity generation, even if there is no physical contact between the FEP and the Al in some of the following operation cycles. To further enhance the triboelectric charge density through nanostructures, the FEP surface is etched by the inductive coupling plasma (ICP) reactive ion etching to create the nanowire-structures (Figure 1b),[33] which helps to increase the surface roughness as well as the effective surface area. As shown in the scanning electron microscopy (SEM) image (Figure 1c), these vertically aligned nanowires have an average diameter of ~100 nm and a length of ~1 μm.

As a result of the triboelectrification, the total amount of negative triboelectric charges on these two pieces of FEP films attached to the two surfaces of the resonator should ideally be the same with the positive charges in the electrode loop composed by the two Al plates. When the negatively charged resonator vibrates between the two electrodes, the positive charges in the electrode loop will be induced to transfer back and forth through the external load, as shown in Figure 1d. This electricity generation process can be described in details as follows. When the resonator gets into contact with the top Al plate (as shown in Figure 1d(I)), all of the positive charges will be attracted to this top electrode (assuming that the distance between the two electrodes is much larger than the thickness of the resonator plate). Subsequently, when this negatively charged resonator vibrates downward from the top Al to the bottom Al, the top electrode will be induced to have a higher potential compared to the bottom electrode, which will drive the positive charges in the electrode loop to transfer through the external load in the same direction with the resonator's movement. This generates a transient current flow (Figure 1d(II)). Once the resonator reaches the bottom Al, all of the positive charges will be then present at this bottom electrode, as shown in Figure 1d(III). Subsequently, the reversed movement of the resonator will lead to a reversed transfer of the positive charges as the second current peak through the external load (Figure 1d(IV)). Until the resonator reaches the status shown in Figure 1d(I), a full cycle is complete.

This electricity generation process of the CF-TENG and its basic characteristics can be theoretically studied and illustrated using the finite-element method. With different positions of the resonator, we first used the COMSOL package to simulate the change of the induced potential difference (*i.e.*, the driving force of the electricity generation) between the two electrodes under the open-circuit condition, with the results shown in Figure 2a. Both the surfaces of the resonator have been assigned with evenly distributed negative charges with an amount of 10 nC, while the same amount of positive charges assigned on each of the two electrodes. As shown in Figure 2a(I), when the resonator is at the middle position in the gap, the two electrodes are in the same potential. If the resonator starts to move downward thus leading to a smaller distance with the bottom electrode, a more negative potential will be induced at the bottom electrode with regard to the top electrode (as shown in Figure 2a(II)). When the resonator gets into contact with the bottom electrode, this induced potential difference will be further increased (Figure 2a(III)). Then, in the next half cycle, the upward movement will bring the resonator into contact with the top electrode, which will fully reverse the induced potential

distribution (Figure 2a(IV)). Thus, from the periodic vibration of the resonator, the reversing potential difference across the two electrodes provides the driving force for the alternating current in the external load. Furthermore, through using the COMSOL to simulate the induced potential differences (*i.e.*, the open-circuit voltage) under a series of different positions of the resonator, we can find that the V_{OC} of the CF-TENG has a linear relationship with the position change of the resonator, as shown in Figure 2b. On the other hand, the simulated short-circuit charge transfer (ΔQ_{SC}) between the two electrodes also has a linear dependence on the moving distance of the resonator. Thus, the electricity generation behavior of the CF-TENG has a very good linearity to the relative position of the electrostatically charged resonator.

This linear characteristic of the CF-TENG can be understood through the analytical studies. The model for the CF-TENG with all the designated parameters is shown in Supporting Information Figure S1. The triboelectric charge density on both surfaces of the resonator is assumed as $-\sigma_0$. The charge densities on the two electrodes are assumed as $+\sigma_1$ and $+\sigma_2$, respectively. Since all the charges in the CF-TENG are generated by the triboelectrification, the following relationship will be satisfied:

$$\sigma_1 + \sigma_2 = 2\sigma_0 \tag{1}$$

Under the open-circuit condition, the charge distribution (*i.e.*, σ_1 and σ_2) between the two electrodes can be arbitrary. Through analytical derivation (with detailed process shown in the Supporting Information), the V_{OC} between the two electrodes can be obtained as

$$V_{OC} = \frac{2\sigma_0}{\varepsilon_0}x - (D-d)\frac{\sigma_1}{\varepsilon_0} + \frac{d}{\varepsilon_0\varepsilon_r}(\sigma_0 - \sigma_1) \tag{2}$$

where D is the distance between the two Al electrodes, d is the thickness of the resonator plate (the thickness of the triboelectric layer is ignored), ε_0 is the vacuum permittivity, ε_r is the relative permittivity of the resonator's supporting substrate (*i.e.*, acrylic in this experimental demonstration), and x is the distance between the resonator and the bottom electrode. Thus, when the resonator moves with a distance of Δx, the change of the V_{OC} should be

$$\Delta V_{OC} = \frac{2\sigma_0}{\varepsilon_0}\Delta x \tag{3}$$

This equation clearly shows the linear characteristics on the V_{OC}, in which the slope is only a function of σ_0, but not dependent on the arbitrary charge distribution between the two electrodes, which is very different from the contact-mode TENGs.[30] Thus, the peak-to-peak value of the V_{OC} ($V_{OC\text{-}p\text{-}p}$) is proportional to the vibration amplitude (A) of the resonating plate, as

$$V_{OC\text{-}p\text{-}p} = \frac{4\sigma_0}{\varepsilon_0}A \tag{4}$$

On the basis of the proportional relationship between the agitated vibration amplitude of the resonating plate and the external vibration amplitude (U_z) on the CF-TENG (the detailed discussion is in Supporting Information), the linear relationship also exists between the $V_{OC\text{-}p\text{-}p}$ and the U_z:

$$V_{OC\text{-}p\text{-}p} = \frac{4\sigma_0}{\varepsilon_0 k\sqrt{(1-r^2)^2 + (2\xi r)^2}}U_z \tag{5}$$

where k is the elastic constant of the spring system (which equals to $2k_0$ in this CF-TENG structure, k_0 is the elastic constant of each individual spring), $r = \omega/\omega_0$, ω_0 is the frequency characteristics of the spring mass, ω is the excitation frequency, and ξ is the primary suspension damping characteristic. This linear relationship serves as the basis for the CF-TENG to quantitatively measure the vibration amplitude.

On the other hand, when the CF-TENG is at the short-circuit (SC) condition in which the voltage between the two electrodes is zero, the equilibrium value of σ_1 can be obtained as

$$\sigma_1 = \frac{2\varepsilon_r\sigma_0}{\varepsilon_r(D-d)+d}x + (D-d)\frac{\sigma_0 d}{\varepsilon_r(D-d)+d} \tag{6}$$

Thus, the ΔQ_{SC} from the resonator's moving distance Δx will be

$$\Delta Q_{SC} = \Delta\sigma_1 \cdot A = \frac{2\varepsilon_r\sigma_0 A}{\varepsilon_r(D-d)+d}\Delta x \tag{7}$$

where A is the surface area of the electrode. Therefore, this equation reveals that the charge transfer in the form of current also has the linear characteristics. Furthermore, the expression for the short-circuit current (I_{SC}) can be obtained as

$$I_{SC} = \frac{dQ_{SC}}{dt} = \frac{2\varepsilon_r\sigma_0 A}{\varepsilon_r(D-d)+d}\cdot\frac{dx}{dt} = \frac{2\varepsilon_r\sigma_0 A}{\varepsilon_r(D-d)+d}v \tag{8}$$

Thus, the I_{SC} is proportional to the instantaneous velocity (v) of the resonator plate in the CF-TENG.

All these unique characteristics of the CF-TENG's electricity generation behavior were experimentally verified through using a linear motor to guide the movement of the resonator plate between the two electrodes. In this way, the mode and parameters of the resonator's movement can be accurately controlled. In the first group of experiments, the linear motor was set to have a cyclic constant-velocity motion between the two electrodes, with the position-time curve shown in Figure 3a(I). As can be seen from Figure 3a(II),(III), both the profiles of the generated V_{OC} and ΔQ_{SC} are triangle waves, which are similar to the position curve with the same phase and period. Through plotting the $V_{OC}/\Delta Q_{SC}$ together with the corresponding position, their characteristics of linearity can be clearly observed, as shown in Figure 3b. With

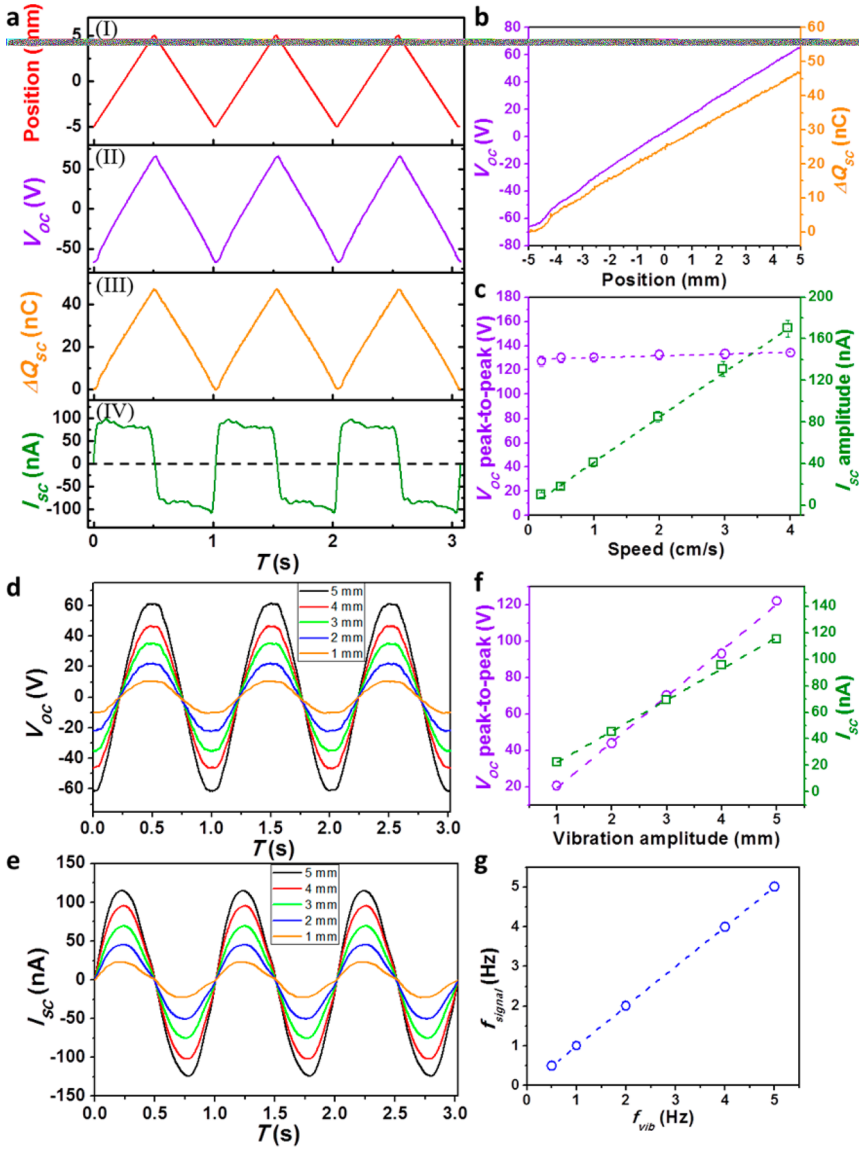

Figure 3. Experimental study of the CF-TENG's electricity generation behavior by using a linear motor to directly drive the movement of the resonator plate. (a) Position curve of the resonator (I), V_{OC} curve (II), ΔQ_{SC} curve (III), and short-circuit current (I_{SC}) curve (IV), when the linear motor was set to a cyclic constant-velocity motion. (b) Plots showing both the relationships between the $V_{OC}/\Delta Q_{SC}$ and the corresponding position of the resonator. (c) Peak-to-peak values of V_{OC} and amplitudes of I_{SC} when the contact-velocity motion of the motor was set to different velocities. (d) Five groups of V_{OC} profiles when the motor was set to sinusoidal motions with the same frequency (1 Hz) but five different amplitudes. (e) Five groups of I_{SC} profiles when the motor was set to sinusoidal motions with the same frequency (1 Hz) but five different amplitudes. (f) Plots showing both the relationships between the peak-to-peak value of V_{OC}, the amplitude of I_{SC} and the resonator plate's sinusoidal vibration amplitude. (g) Relationship between the frequency of the electrical signals from the CF-TENG and the vibration frequency of the resonator plate.

the constant velocity during the movement, the profile of the I_{SC} is close to the square wave, in which the symmetric amplitude should directly reflect the velocity of the resonator. We further investigated the influence of the moving speed of the resonator on the electric signal from the CF-TENG, by setting the motor to a series of different speeds between 0 and 4 cm/s. As can be seen from Figure 3c, the amplitude of the I_{SC} increases almost linearly with the speed, while the peak-to-peak value of the V_{OC} remains constant. These are in accordance with the theoretical relationships in eqs 3 and 8. Therefore, the instantaneous value of the I_{SC} can serve as a quantitative sensing signal for the instantaneous velocity of the resonator in the CF-TENG.

In the second group of experiments, the linear motor was set to follow sinusoidal motions. Because of the linearity in the electricity generation behavior, the profiles of V_{OC} (Figure 3d), ΔQ_{SC} (Supporting Information Figure S2) and I_{SC} (Figure 3e) are all sinusoidal waves, but with a $\pi/2$ phase shift. When the vibration amplitude of the resonator was set to 5 evenly spaced values between 0 and 5 mm while maintaining the same frequency of 1 Hz, both the amplitudes of the V_{OC}

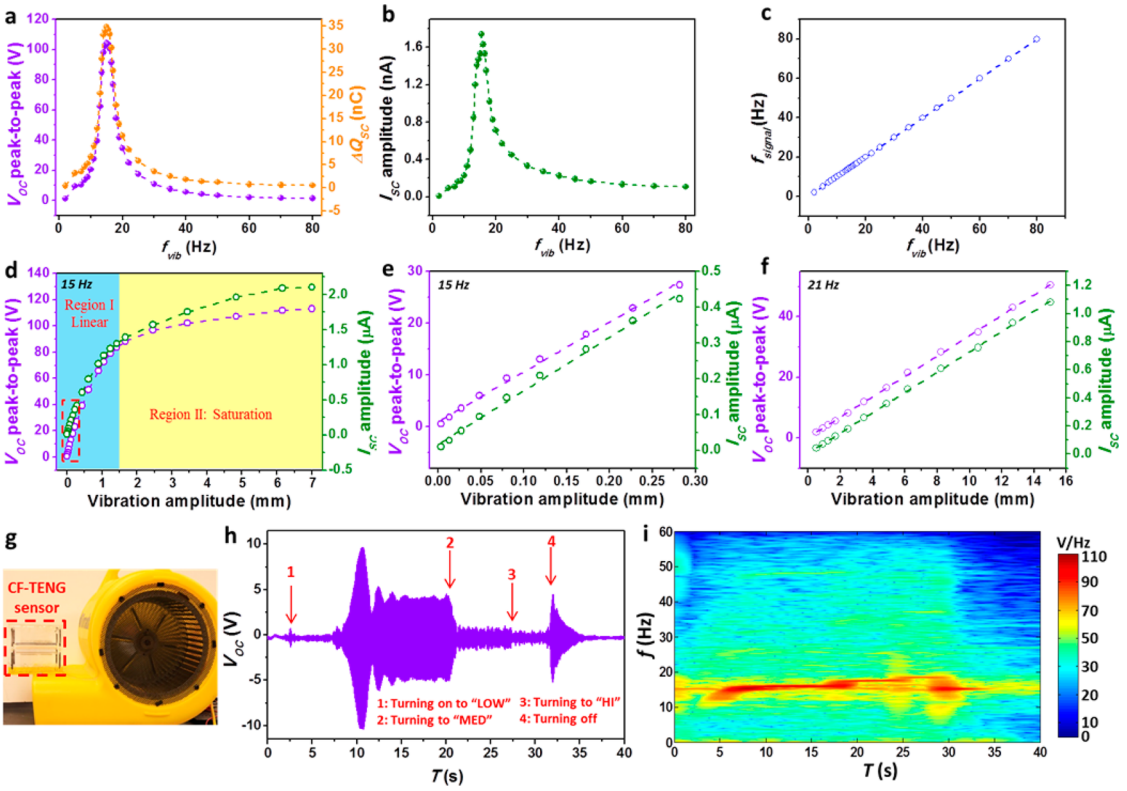

Figure 4. Electrical output of the CF-TENG as a self-powered vibration sensor when it is attached to an external vibration source. (a) V_{OC} and ΔQ_{SC}, (b) I_{SC} from the CF-TENG when it was triggered by vibrations with different frequencies but the same amplitude. (c) Plot showing the relationship between the frequency of the electrical signals from the CF-TENG and the frequency of the external vibration source. (d) V_{OC} and I_{SC} from the CF-TENG triggered by vibrations with different amplitudes, when the external vibration source is at the resonating frequency (15 Hz) of the CF-TENG. (e) Enlarged plot of panel d with the vibration amplitude in the range below 0.3 mm. (f) V_{OC} and I_{SC} from the CF-TENG triggered by vibrations with different amplitudes, when the external vibration source is not at the resonating frequency of the CF-TENG. (g) Photograph showing the demonstration of using the CF-TENG to monitor the vibration of a wind blower during its operation. (h) V_{OC} from the CF-TENG when the wind blower was sequentially switched to different speeds. (i) Short-time Fourier transform of the V_{OC} signal shown in panel h.

(Figure 3d) and the ΔQ_{SC} (Supporting Information Figure S2) change in the same scale with the vibration amplitude, which can be expected from their relationships with Δx shown in eqs 3 and 7. On the other hand, since the change of the sinusoidal vibration amplitude under the same frequency will lead to the change of the maximum velocity, the amplitude of the I_{SC} also changes proportionally (Figure 3e). When the peak-to-peak values of the V_{OC} and the amplitudes of the I_{SC} are plotted in the same figure with the corresponding vibration amplitude (Figure 3f), their linear relationships can be observed very clearly. This unique characteristic makes the CF-TENG distinctively different from the contact-mode TENG whose effective electricity generation only takes place when the gap distance is within the small range. It gives the CF-TENG the good superiorities not only for sensing the vibration amplitudes, but also for harvesting vibrational energy with very board effective amplitude. Besides the amplitude, the frequency is the other important parameter for vibrations. The electrical output of the CF-TENG was measured when the sinusoidal motion of the resonator was set to different frequencies while maintaining the same amplitude of 5 mm. As can be seen in Figure 3g, the frequency of the obtained electrical signals (V_{OC}, ΔQ_{SC}, and I_{SC}) accurately reflects the frequency of the vibration, which clearly reveals the CF-TENG's capability of actively measuring the vibration frequency.

When the CF-TENG with the resonator plate supported by springs (as shown in Figure 1a) is bonded to a vibration source, the resonator plate will be triggered to vibrate between the two electrodes, which will generate electrical output with the above-demonstrated linear characteristic as long as the resonator plate is triboelectrically charged. In the experimental testing of its sensing capability, an electrodynamic shaker was employed as the vibration source, which can generate sinusoidal output with controlled amplitude and frequency. It needs to be noticed that in order to achieve the linearity in the electricity generation it is very important to reach a good alignment between the direction of the external vibration and the vertical axis of the CF-TENG. First, the electrical output was measured under a series of different frequencies ranging between 5 and 80 Hz but with the same amplitude of 10 mm. As shown in Figure 4a,b, the V_{OC}, ΔQ_{SC}, and I_{SC}

all reach their maximum values at ~15 Hz. Thus, it should be the resonant frequency of the CF-TENG, at which the resonator plate reaches the largest vibration distance under the same external vibration amplitude. From Figure 4a, it can be also found that the detailed trends of the V_{OC} and the ΔQ_{SC} are exactly the same, which reflects the proportional relationship between them as revealed by eqs 3 and 7. Besides the amplitudes of the electrical signals, the most direct response of the change in the vibration frequency is the frequency of the electrical signals, as shown in Figure 4c. Thus, with the use of the CF-TENG as the active sensor, the frequency of the vibration source can be instantaneously monitored through the frequency analysis of the electrical signals.

As stated previously, a good linearity in the electricity generation behavior gives the CF-TENG the supreme capability of quantitatively sensing the amplitude of the vibration. To experimentally demonstrate this, the electrical signals of the CF-TENG were measured under a series of different vibration amplitudes but with the frequency maintained the same. In the first set of experiment, the frequency was set to the resonant frequency of the CF-TENG, which will give the resonator plate the largest vibration distance/amplitude. As shown in Figure 4d, when the vibration amplitude of the shaker is within the small range (below 1.5 mm, *i.e.*, Region I shown in Figure 4d), both the peak-to-peak value of the V_{OC} and the amplitude of the I_{SC} increase almost linearly with the increase of the vibration amplitude. This response comes from the linear relationship between the agitated vibration amplitude of the resonator plate and the vibration amplitude of the entire CF-TENG. However, when the vibration amplitude is above ~1.5 mm, the resonator plate will start to get into contact with the two electrode plates, which will limit the further increase of the vibration distance of the resonator plate. This results in the saturation behavior of the electrical outputs at relatively large vibration amplitudes (Region II shown in Figure 4d). Thus, in order to get the reliable results for the vibration amplitude, it is important to make sure the CF-TENG operating below its saturation threshold. Moreover, from Figure 4e as the enlarged plot of the curves in Figure 4d below the vibration amplitude of 0.3 mm, it can be found that both the V_{OC} and the I_{SC} have very good linear responses. When the vibration amplitude is only 3.5 μm, the peak-to-peak value of the V_{OC} and the amplitude of the I_{SC} generated by the CF-TENG are still 0.54 V and 10 nA, which are far higher than the measurable limits of most preamplifiers. Therefore, when the vibration source is at or close to the resonant frequency of the CF-TENG, it has an extremely high sensitivity for very subtle vibrations. In the other group of experiments, the relationship between the electrical signals and the vibration amplitude was measured at a frequency of 21 Hz, which is off the resonant frequency. As shown in Figure 4f, when the vibration amplitude is increased up to 15 mm (the largest vibration amplitude that can be provided by the shaker), both the V_{OC} and the I_{SC} follow very good linear behaviors. Thus, when the vibration source is not at the resonant frequency of the CF-TENG, this active sensor has the capability of quantitatively measuring the amplitude in a wide range. Similarly, the CF-TENG's responses to the vibration amplitude at the entire frequency range can be calibrated following the above method. When the CF-TENG is used as the active sensor for an external vibration source, its vibration frequency can be first obtained through the frequency analysis of the electrical signal, and then the vibration amplitude can be acquired from the calibration curve for this same frequency. Since the linear relationship between the input vibration amplitude and the electrical output only exists below the saturation threshold for the CF-TENG, it is important to make sure the CF-TENG always operates under this threshold. It should be noted that although the quantitative measurement of the vibration amplitude requires the noncontact mode operation of the CF-TENG, the contact mode operation needs to be enabled occasionally or purposely initiated in the first few cycles to generate the triboelectric charges on the dielectric surfaces of the resonating plate. And when an electret material (*e.g.*, FEP in this paper) is utilized as the dielectric surface for the resonating plate, the generated triboelectric charges can be preserved quasi-permanently,[34,35] so that its density can remain almost constant over a long time. This gives the CF-TENG a very stable relationship between its electrical output and the input vibration amplitude (Supporting Information Figure S3) for the quantitative measurement.

As a demonstration of the CF-TENG's outstanding capability in vibration sensing, it was mounted onto a wind blower to monitor its vibration during the operation (Figure 4g and Supporting Information Video S1). When the wind blower was sequentially turned on from the "off" state to the "LOW" speed, then turned to the "MED" speed, then to the "HIGH" speed, and finally turned off, the V_{OC} signal generated by the CF-TENG is shown in Figure 4h. From the short-time Fourier transform (STFT) of the V_{OC} signal, the instantaneous frequency distribution of the wind blower throughout this operation process can be obtained in Figure 4i. It clearly shows that when the wind blower was running at the "LOW" speed, its frequency was mainly around 15 Hz, which is just the resonant frequency of the CF-TENG. Then, when the wind blower was sequentially turned to "MED" and "HIGH", the frequency changed to ~18 and ~20 Hz, respectively. Finally, when it was turned off, the frequency temporarily went back to ~15 Hz before it fully stopped. In each stage with the same frequency, the change of the amplitude in the V_{OC} signal directly reflects the change of the

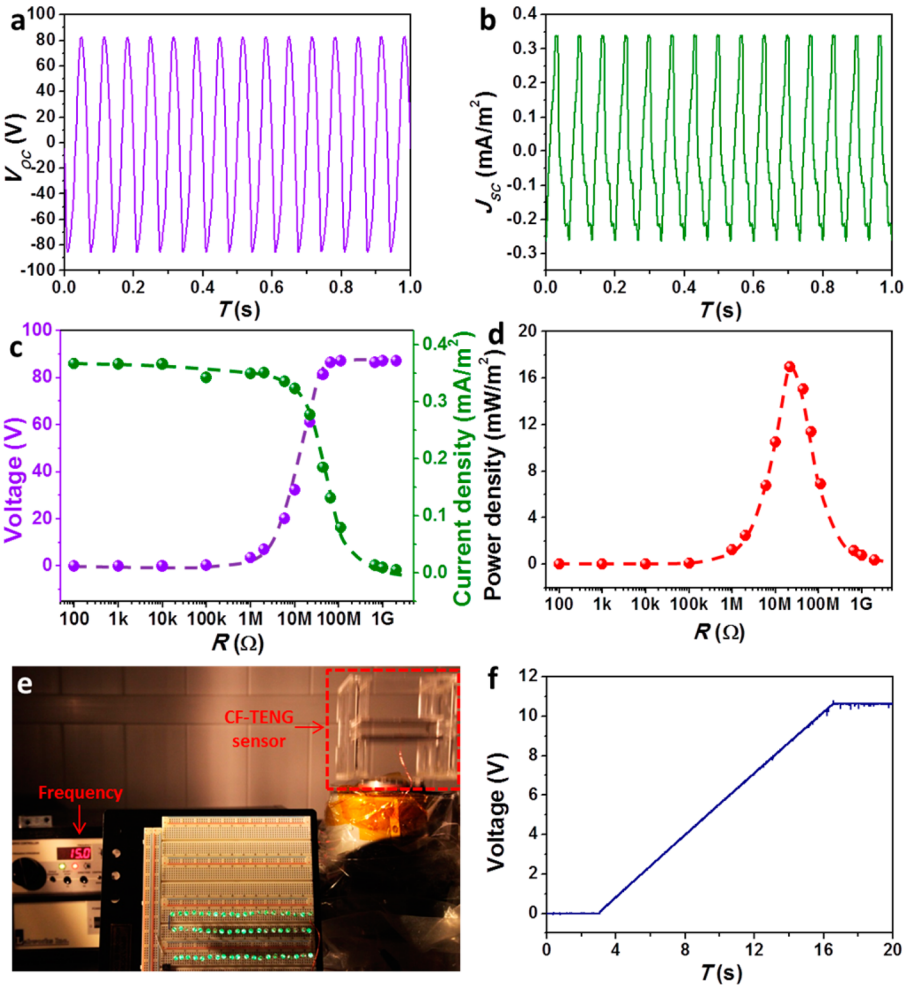

Figure 5. Performance of the CF-TENG when it serves as an energy harvester for the vibration with the amplitude of 1.5 cm and the frequency of 15 Hz. (a) Output V_{OC}, and (b) output short-circuit current density (J_{SC}) of the CF-TENG. (c) Voltage and current density obtained by the load with different resistances. (d) Power density obtained by the load with different resistances. (e) 60 LEDs instantaneously driven by the CF-TENG. (f) Storage of the electricity generated by the CF-TENG in a 14.7-μF capacitor.

vibration amplitude of the wind-blower, as shown in Figure 4h. Therefore, this demonstration convincingly shows the CF-TENG's supreme capability in quantitatively detecting both the amplitude and the frequency of any arbitrary vibration.

The CF-TENG can also work as an energy harvesting device for the environmental vibration, when the generated electricity is utilized to power other electronic devices/systems. Under the condition that the vibration source has the amplitude of 1.5 cm and the frequency of 15 Hz (*i.e.*, the resonant frequency of the CF-TENG), a continuous AC output is generated. The V_{OC} has a peak-to-peak value of 165 V (Figure 5a), while the short-circuit current density (J_{SC}) reaches 0.35 mA/m^2 amplitude (Figure 5b). Once the CF-TENG is connected to an external load, the current density obtained by the load decreases as the load resistance increases, while the voltage shows a rising trend (Figure 5c). The power density received by the load reaches the maximum value of 17 mW/m^2 at the load resistance of 20 MΩ (Figure 5d). This generated electricity can directly drive 60 commercial light-emitting diodes (LEDs) simultaneously, as shown in Figure 5e and Supporting Information Video S2. Owing to the linearity in the electricity generation behavior, the physical contact between the triboelectrically charged resonator and the electrodes is not mandatory for the effective mechanical energy conversion. As can be seen in Supporting Information Video S2, when the vibration amplitude of the shaker is gradually tuned down to a much smaller value, these LEDs still can be lit up by the CF-TENG. Similarly with the sliding-based freestanding-TENG, the CF-TENG's capability of noncontact operation also brings about the advantages of improved energy conversion efficiency and better stability. Besides directly driving electronics, the electricity generated by the CF-TENG can also be stored in energy storage units (such as batteries or capacitors) in order to get a regulated power. As shown in Figure 5f, the CF-TENG under the above-described vibration condition can charge a 1.47-μF capacitor from empty to 10.5 V in only 13.5 s.

CONCLUSIONS

In summary, we first demonstrated a vertical contact-separation based freestanding triboelectric nanogenerator (CF-TENG), which can effectively convert vibrational motions into electricity. This unique TENG structure and operation mode has been shown to have a supreme linearity in the electricity generation behavior, both through the theoretical analysis, and through the experimental measurement when the triboelectric resonator is driven by a linear motor in a controllable and tunable manner. Because of this unique characteristic, the amplitudes of the generated electric signals (both V_{OC} and I_{SC}) are proportional to the amplitude of the vibration under the same frequency. Thus, the CF-TENG is developed as the first triboelectrification-based self-powered vibration sensor that can quantify the amplitude, as well as the frequency. When the CF-TENG works at its resonant frequency, it can effectively sense very subtle vibrations (with the amplitude as low as 3.5 μm in the experimental demonstration using a CF-TENG with the electrode size of 10 cm $\times$ 10 cm and the electrode gap of 2 cm). Furthermore, the CF-TENG can also work as the energy harvester for the vibrational energy, providing the sustainable power source for electronic systems. This work not only further completes the family of the TENG's basic modes, but also broadens the applications of TENGs as active sensors and energy harvesters.

EXPERIMENTAL SECTION

Fabrication of the Nanowire Array on the Surface of FEP Film. The FEP film (with the thickness of 50 μm) was first rinsed with menthol, isopropyl alcohol, and deionized water, consecutively, and then blown dry with nitrogen gas. Subsequently, a thin layer of Au with a thickness of 10 nm was sputtered onto the FEP surface as the mask for the etching process. Then the inductively coupled plasma (ICP) reactive ion etching was used to produce the aligned nanowires on the surface. Specifically, Ar, O_2 and CF_4 gases were introduced into the ICP chamber with the flow ratio of 15.0, 10.0, and 30.0 sccm, respectively. The first power source of 400 W was used to generate a large density of plasma and the other power of 100 W was used to accelerate the plasma ions. The FEP film was etched for 60 s.

Fabrication of the CF-TENG. The skeleton of the CF-TENG is constructed by acrylic sheet with the thickness of 1/8 in. First, the acrylic sheet was carved by a laser cutter machine to form desired shapes. Then they were glued together using epoxy to form the rectangular bracket. Two acrylic plates with the size of 10 cm $\times$ 10 cm were sequentially deposited with 30 nm Cr and 100 Al as the two electrodes. Then they were supported by additional acrylic sheets from the two ends of the bracket, with the parallel configuration and a distance of 20 mm. Next, a 1/16 in. thick acrylic sheet was cut into the size of 10 cm $\times$ 10 cm with 4 extended corners to serve as the resonator. On both of its two surfaces, two pieces of ICP-etched FEP films (with the size of 10 cm $\times$ 10 cm) were laminated with the nanowire-covered side facing outward. Then, the resonator plate was connected by 8 springs from its four extended corners to the two ends of the bracket.

Conflict of Interest: The authors declare no competing financial interest.

Supporting Information Available: The detailed derivation of the open-circuit voltage, the schematic diagram showing the parameters of the CF-TENG model, and the Q_{SC} profiles when the motor was set to sinusoidal motions with the same frequency (1 Hz) but five different amplitudes. This material is available free of charge *via* the Internet at http://pubs.acs.org.

Acknowledgment. This work was supported by Basic Energy Sciences DOE, MURI from Airforce, the Hightower Chair foundation, and the "thousands talents" program for pioneer researcher and his innovation team.

REFERENCES AND NOTES

1. Ashraf, K.; Khir, M. H. M.; Dennis, J. O.; Baharudin, Z. Improved Energy Harvesting from Low Frequency Vibrations by Resonance Amplification at Multiple Frequencies. *Sens. Actuators, A* **2013**, *195*, 123–132.
2. Beeby, S. P.; Torah, R. N.; Tudor, M. J.; Glynne-Jones, P.; O'Donnell, T.; Saha, C. R.; Roy, S. A Micro Electromagnetic Generator for Vibration Energy Harvesting. *J. Micromech. Microeng.* **2007**, *17*, 1257–1265.
3. Ramsay, M. J.; Clark, W. W. Piezoelectric Energy Harvesting for Bio MEMS Applications. In *Smart Structures and Materials 2001: Industrial and Commercial Applications of Smart Structures Technologies*; SPIE: Bellingham, WA, 2001; Vol. 4332, 429–438.
4. Rome, L. C.; Flynn, L.; Goldman, E. M.; Yoo, T. D. Generating Electricity while Walking with Loads. *Science* **2005**, *309*, 1725–1728.
5. Bernstein, J.; Miller, R.; Kelley, W.; Ward, P. Low-Noise MEMS Vibration Sensor for Geophysical Applications. *J. Microelectromech. Syst.* **1999**, *8*, 433–438.
6. Gabrielson, T. B. Mechanical-Thermal Noise in Micromachined Acoustic and Vibration Sensors. *IEEE Trans. Electron Devices* **1993**, *40*, 903–909.
7. Gangopadhyay, T. K. Prospects for Fibre Bragg Gratings and Fabry-Perot Interferometers in Fibre-Optic Vibration Sensing. *Sens Actuators, A* **2004**, *113*, 20–38.
8. Itakura, Y.; Fujii, N.; Sawada, T. Basic Characteristics of Ground Vibration Sensors for the Detection of Debris Flow. *Phys. Chem. Earth, B* **2000**, *25*, 717–720.
9. Kamata, M.; Obara, M.; Gattass, R. R.; Cerami, L. R.; Mazur, E. Optical Vibration Sensor Fabricated by Femtosecond Laser Micromachining. *Appl. Phys. Lett.* **2005**, *87*, No. 051106.
10. Yu, A. F.; Jiang, P.; Wang, Z. L. Nanogenerator as Self-powered Vibration Sensor. *Nano Energy* **2012**, *1*, 418–423.
11. Fan, F. R.; Tian, Z. Q.; Wang, Z. L. Flexible Triboelectric Generator!. *Nano Energy* **2012**, *1*, 328–334.
12. Wang, S. H.; Lin, L.; Wang, Z. L. Nanoscale Triboelectric-Effect-Enabled Energy Conversion for Sustainably Powering Portable Electronics. *Nano Lett.* **2012**, *12*, 6339–6346.
13. Zhu, G.; Zhou, Y. S.; Bai, P.; Meng, X. S.; Jing, Q. S.; Chen, J.; Wang, Z. L. A Shape-Adaptive Thin-Film-Based Approach for 50% High-Efficiency Energy Generation Through Micro-Grating Sliding Electrification. *Adv. Mater.* **2014**, *26*, 3788–3796.
14. Tang, W.; Meng, B.; Zhang, H. X. Investigation of Power Generation Based on Stacked Triboelectric Nanogenerator. *Nano Energy* **2013**, *2*, 1164–1171.
15. Yang, Y.; Zhang, H. L.; Chen, J.; Jing, Q. S.; Zhou, Y. S.; Wen, X. N.; Wang, Z. L. Single-Electrode-Based Sliding Triboelectric Nanogenerator for Self-Powered Displacement Vector Sensor System. *ACS Nano* **2013**, *7*, 7342–7351.
16. Lin, L.; Wang, S. H.; Xie, Y. N.; Jing, Q. S.; Niu, S. M.; Hu, Y. F.; Wang, Z. L. Segmentally Structured Disk Triboelectric Nanogenerator for Harvesting Rotational Mechanical Energy. *Nano Lett.* **2013**, *13*, 2916–2923.
17. Wang, S. H.; Xie, Y. N.; Niu, S. M.; Lin, L.; Wang, Z. L. Freestanding Triboelectric-Layer Based Nanogenerators

for Harvesting Energy from a Moving Object or Human Motion in Contact and Non-Contact Modes. *Adv. Mater.* **2014**, *26*, 2818–2824.
18. Wang, S. H.; Lin, Z. H.; Niu, S. M.; Lin, L.; Xie, Y. N.; Pradel, K. C.; Wang, Z. L. Motion Charged Battery as Sustainable Flexible-Power-Unit. *ACS Nano* **2013**, *7*, 11263–11271.
19. Baytekin, H. T.; Baytekin, B.; Hermans, T. M.; Kowalczyk, B.; Grzybowski, B. A. Control of Surface Charges by Radicals as a Principle of Antistatic Polymers Protecting Electronic Circuitry. *Science* **2013**, *341*, 1368–1371.
20. Baytekin, H. T.; Baytekin, B.; Incorvati, J. T.; Grzybowski, B. A. Material Transfer and Polarity Reversal in Contact Charging. *Angew. Chem., Int. Ed.* **2012**, *51*, 4843–4847.
21. Soh, S.; Kwok, S. W.; Liu, H.; Whitesides, G. M. Contact De-electrification of Electrostatically Charged Polymers. *J. Am. Chem. Soc.* **2012**, *134*, 20151–20159.
22. Lin, L.; Xie, Y. N.; Wang, S. H.; Wu, W. Z.; Niu, S. M.; Wen, X. N.; Wang, Z. L. Triboelectric Active Sensor Array for Self-Powered Static and Dynamic Pressure Detection and Tactile Imaging. *ACS Nano* **2013**, *7*, 8266–8274.
23. Zhou, Y. S.; Zhu, G.; Niu, S. M.; Liu, Y.; Bai, P. S.; Jing, Q.; Wang, Z. L. Nanometer Resolution Self-Powered Static and Dynamic Motion Sensor Based on Micro-Grated Triboelectrification. *Adv. Mater.* **2014**, *26*, 1719–1724.
24. Yang, W. Q.; Chen, J.; Jing, Q. S.; Yang, J.; Wen, X. N.; Su, Y. J.; Zhu, G.; Bai, P.; Wang, Z. L. 3D Stack Integrated Triboelectric Nanogenerator for Harvesting Vibration Energy. *Adv. Funct. Mater.* **2014**, *24*, 4090–4096.
25. Yang, J.; Chen, J.; Yang, Y.; Zhang, H. L.; Yang, W. Q.; Bai, P.; Su, Y. J.; Wang, Z. L., Broadband Vibrational Energy Harvesting Based on a Triboelectric Nanogenerator. *Adv. Energy Mater.* **2014**, *4*.10.1002/aenm.201301322
26. Chen, J.; Zhu, G.; Yang, W. Q.; Jing, Q. S.; Bai, P.; Yang, Y.; Hou, T. C.; Wang, Z. L. Harmonic-Resonator-Based Triboelectric Nanogenerator as a Sustainable Power Source and a Self-Powered Active Vibration Sensor. *Adv. Mater.* **2013**, *25*, 6094–6099.
27. Yang, W. Q.; Chen, J.; Zhu, G.; Yang, J.; Bai, P.; Su, Y. J.; Jing, Q. S.; Cao, X.; Wang, Z. L. Harvesting Energy from the Natural Vibration of Human Walking. *ACS Nano* **2013**, *7*, 11317–11324.
28. Yang, W. Q.; Chen, J.; Zhu, G.; Wen, X. N.; Bai, P.; Su, Y. J.; Lin, Y.; Wang, Z. L. Harvesting Vibration Energy by a Triple-Cantilever Based Triboelectric Nanogenerator. *Nano Res.* **2013**, *6*, 880–886.
29. Hu, Y. F.; Yang, J.; Jing, Q. S.; Niu, S. M.; Wu, W. Z.; Wang, Z. L. Triboelectric Nanogenerator Built on Suspended 3D Spiral Structure as Vibration and Positioning Sensor and Wave Energy Harvester. *ACS Nano* **2013**, *7*, 10424–10432.
30. Niu, S. M.; Wang, S. H.; Lin, L.; Liu, Y.; Zhou, Y. S.; Hu, Y. F.; Wang, Z. L. Theoretical Study of Contact-Mode Triboelectric Nanogenerators as an Effective Power Source. *Energy Environ. Sci.* **2013**, *6*, 3576–3583.
31. Lin, L.; Wang, S. H.; Niu, S. M.; Liu, C.; Xie, Y. N.; Wang, Z. L. Non-Contact Free-Rotating Disk Triboelectric Nanogenerator as a Sustainable Energy Harvester and Self-Powered Mechanical Sensor. *ACS Appl. Mater. Interfaces* **2014**, *6*, 3031–3038.
32. Xie, Y. N.; Wang, S. H.; Niu, S. M.; Lin, L.; Jing, Q. S.; Yang, J.; Wu, Z. Y.; Wang, Z. L. Grating-Structured Freestanding Triboelectric-Layer Nanogenerator for Harvesting Mechanical Energy at 85% Total Conversion Efficiency. *Adv. Mater.* **2014**, *26*, 6599–6607.
33. Fang, H.; Wu, W. Z.; Song, J. H.; Wang, Z. L. Controlled Growth of Aligned Polymer Nanowires. *J. Phys. Chem. C* **2009**, *113*, 16571–16574.
34. Jacobs, H. O.; Whitesides, G. M. Submicrometer Patterning of Charge in Thin-Film Electrets. *Science* **2001**, *291*, 1763–1766.
35. Wang, S. H.; Xie, Y. N.; Niu, S. M.; Lin, L.; Liu, C.; Zhou, Y. S.; Wang, Z. L. Maximum Surface Charge Density for Triboelectric Nanogenerators Achieved by Ionized-Air Injection: Methodology and Theoretical Understanding. *Adv. Mater.* **2014**, *26*, 6720–6728.